Pharmacophore Based Receptor Modeling: The Case of Adenosine A₃ Receptor Antagonists. An Approach to the Optimization of Protein Models

Andrea Tafi,[†] Cesare Bernardini,[†] Maurizio Botta,*,[†] Federico Corelli,[†] Matteo Andreini,[‡] Adriano Martinelli,*,[‡] Gabriella Ortore,[‡] Pier Giovanni Baraldi,*,[§] Francesca Fruttarolo,[§] Pier Andrea Borea,[#] and Tiziano Tuccinardi[‡]

Dipartimento Farmaco Chimico Tecnologico, Università degli Studi di Siena, Via A. Moro, 53100 Siena, Italy, Dipartimento di Scienze Farmaceutiche, Università di Pisa, Via Bonanno 6, 56126 Pisa, Italy, Dipartimento di Scienze Farmaceutiche, Università degli Studi di Ferrara, Via Fossato di Mortara 17-19, 44100 Ferrara, Italy, and Dipartimento di Medicina Clinica e Sperimentale-Sezione di Farmacologia, Università degli Studi di Ferrara, Via Fossato di Mortara 17-19, 44100 Ferrara, Italy

To design and synthesize new potent and selective antagonists of the human A₃ adenosine receptor, pharmacophoric hypotheses were generated with the software Catalyst for a comprehensive set of compounds retrieved from previous literature. Three of these pharmacophores were used to drive the optimization of a molecular model of the receptor built by homology modeling. The alignment of the ligands proposed by Catalyst was then used to manually dock a set of known A₃ antagonists into the binding site, and as a result, the model was able to explain the different binding mode of very active compounds with respect to less active ones and to reproduce, with good accuracy, free energies of binding. The docking highlighted that the nonconserved residue Tyr254 could play an important role for A₃ selectivity, suggesting that a mutagenesis study on this residue could be of interest in this respect. The reliability of the whole approach was successfully tested by rational design and synthesis of new compounds.

Introduction

Adenosine is an ubiquitous neuromodulator that acts by stimulating four cell surface receptors (A₁, A₂A, A₂B, A₃), all being part of the huge family of the G-protein-coupled receptors (GPCRs). In particular, A₃ receptors, discovered in 1992 by Zhuo et al.,[1] have been reported to be activated by a higher concentration of their natural ligand with respect to other subtypes, suggesting a pathophysiological role during hypoxic stress and other cellular damage.[2] While A₃ activation results in general hypotension and mast-cells degranulation,[3,4] selective antagonists of these receptors may be used in clinical practice as anti-inflammatory[5] as well as cerebroprotective[6,7] and anti-asthmatic agents.[8]

In the past decade, because of the importance of this new biological target, a great effort has been made to design and synthesize new potent and selective agonists and antagonists of the human A₃ adenosine receptor (hA₃AR). Because of the lack of experimental 3D structural data about the hA₃AR binding site, the rational design of hA₃AR antagonists has been commonly pursued through the construction of receptor models or, alternatively, by QSAR/3D-QSAR approaches (such as CoMFA) using experimental data obtained by previously synthesized ligands. As a result of all this reseach, several classes of compounds, including pyrazolo[4,3-*e*]-1,2,4-triazolo[1,5-*c*]-pyrimidine derivatives,[9−12] triazoloquinazoline derivatives,[13] isoquinoline and quinazoline analogues,[14−16] and 3,5-diacyl-2,4-dialkylpyridine[17−19] and pyridine derivatives,[20,21] have been synthesized and tested as hA₃AR antagonists.

To design and synthesize a new generation of potent and selective antagonists with improved absorption, distribution, metabolism, and excretion (ADME) profiles as well as increased water solubility compared to previous analogues, we set up a drug design approach, in which ligand-based information and homology modeling were combined throughout to increase the success possibilities. Many studies have been published in which the docking procedure was used as an alignment tool for the development of 3D-QSAR models.[22−24] Furthermore, some recent studies have demonstrated that GPCR models of higher accuracy can be produced if homology modeling, based on the rhodopsin X-ray template, is supported by experimental structural constraints appropriate for active or inactive receptor conformations[25] or if crude models are optimized by including ligand-based information.[26] Regarding this last approach, Klebe and co-workers have recently developed the MOBILE method, where homology models are refined by including information about bioactive ligands as spatial restraints,[26] and have applied it to the discovery of neurokinin-1 receptor antagonists.[27]

In this study we have actually merged the capabilities of two generally complementary computational methodologies, that is, pharmacophore[28] and homology modeling,[29] to build a predictive three-dimensional model of the human A₃ receptor. The aim of our approach was to gain information from a set of ligands by means of a 3D-QSAR methodology to drive the refinement of the receptor model and to increase the probability of identifying the most important features for ligand recognition.

Accordingly, we first generated several common feature hypotheses for human A₃ receptor antagonists and screened the three most promising pharmacophores. These pharmacophores were all characterized by good statistical parameters and prediction ability; moreover, they were very similar in terms of feature composition and disposition in three-dimensional space.
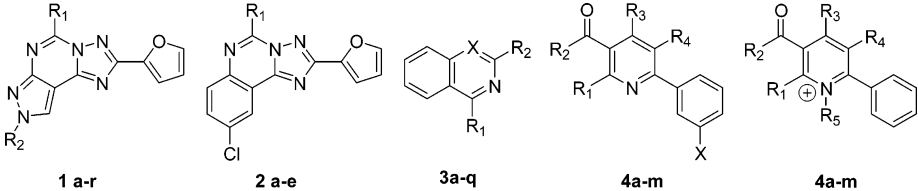
* To whom correspondence should be addressed. For M.B.: phone, +39-577-234306; fax, +39-577-234333; e-mail, botta@unisi.it. For A.M.: phone, +39-50-2219556; fax, +39-50-2219605; e-mail, marti@farm.unipi.it. For P.G.B.: phone, +39-532-291293; fax, +39-532-291296; e-mail, baraldi@unife.it.

[†] Università degli Studi di Siena.
[‡] Università di Pisa.
[§] Dipartimento di Scienze Farmaceutiche, Università degli Studi di Ferrara.
[#] Dipartimento di Medicina Clinica e Sperimentale-Sezione di Farmacologia, Università degli Studi di Ferrara.

Table 1. hA$_3$AR Antagonists Considered for Pharmacophore Generation and Validation

compd	R$_1$	R$_2$	R$_3$	R$_4$	R$_5$	X
1a	NHCONH−(4-SO$_3$H−Ph)	ethyl				
1b	NH$_2$	ethyl				
1c	NHCONH−(3-Cl−Ph)	methyl				
1d	NHCONH-4-CH$_3$−Ph	ethyl				
1e	NHCONH-4-F−Ph	ethyl				
1f	NHCONH−(2-OCH$_3$−Ph)	ethyl				
1g	NHCONH−(2-Cl−Ph)	ethyl				
1h	NHCONH−(3-Cl−Ph)	ethyl				
1i	NHCONH−Ph	methyl				
1j	NHCONH−(4-OCH$_3$−Ph)	ethyl				
1k	NHCONH−4-pyridyl	methyl				
1l[a]	NH$_2$	propyl				
1m[a]	NHCONH−(4-OCH$_3$−Ph)	propyl				
1n[a]	NH$_2$	H				
1o[a]	NHCONH−(4-OCH$_3$−Ph)	methyl				
1p[a]	NHCONH−(4-NO$_2$-Ph)	ethyl				
1q[a]	NHCONH−Ph	propyl				
1r[a]	NHCONH−(4-SO$_3$H−Ph)	propyl				
2a	NH$_2$					
2b	NHCO−Ph					
2c	NHCOCH$_2$−Ph					
2d	NHCOCH$_2$CH$_3$					
2e[a]	NHCOCH$_3$					
3a	NHCO−(4-OCH$_3$−Ph)	2-pyridyl				CH
3b	NHCO−Ph	2-pyridyl				CH
3c	NHCO−(4-CH$_3$−Ph)	2-pyridyl				CH
3d	NHCO−(3,4-CH$_3$−Ph)	2-pyridyl				CH
3e	NHCO−(3,4-OCH$_3$−Ph)	2-pyridyl				CH
3f	NHCO−3Cl−Ph	2-pyridyl				CH
3g	NHCO−3OCH$_3$−Ph	2-pyridyl				CH
3h	NHCONH−Ph	2-pyridyl				CH
3i	NHCONH−Ph	H				N
3j	NHCONH−Ph	2-pyridyl				N
3k	NHCONH−Ph	3-pyridyl				N
3l	NHCONH−Ph	3-CH$_3$−2-pyridyl				N
3m	NHCONH−Ph	*N,N*-diethylamino				N
3n	NHCONH−Ph	1-pyrrolidinyl				N
3o[a]	NHCO−(4-Cl−Ph)	2-pyridyl				CH
3p[a]	NHCO−(2,4-CH$_3$−Ph)	2-pyridyl				CH
3q[a]	NHCO−(3-CH$_3$−Ph)	2-pyridyl				CH
4a	methyl	*O*-ethyl	methyl	COO−ethyl		H
4b	methyl	*O*-propyl	methyl	COO−ethyl		H
4c	methyl	*O*-ethyl	ethyl	COO−ethyl		H
4d	methyl	*O*-ethyl	ethyl	COO−ethyl		H
4e	ethyl	*O*-ethyl	ethyl	COO−ethyl		H
4f	ethyl	*O*-ethyl	ethyl	COO−propyl		H
4g	ethyl	*O*-ethyl	*n*-propyl	COO−propyl		H
4h	ethyl	*O*-propyl	ethyl	COO−propyl		Cl
4i[a]	methyl	*S*-ethyl	methyl	COO−ethyl		H
4j[a]	propyl	*S*-ethyl	ethyl	COO−ethyl		H
4k[a]	methyl	*S*-ethyl	propyl	COO−ethyl		H
4l[a]	ethyl	*S*-ethyl	ethyl	COOCH$_2$CH$_2$OH		H
4m[a]	ethyl	*S*-ethyl	ethyl	COO−ethyl		H
5a	methyl	*O*-ethyl	ethyl	COO−ethyl	methyl	
5b[a]	ethyl	*S*-ethyl	ethyl	COO−ethyl	methyl	

[a] Compounds included in the test set.

At the same time, a raw model of hA$_3$AR was generated by homology modeling, using bovine rhodopsin as a template,[30] and several molecular interaction fields (MIFs) were calculated for each transmembrane helix with the aim of localizing the minimum-energy interaction points.

The three screened pharmacophores were then subjected, one by one, to a manual docking procedure into the raw binding site, which was adjusted as well, to achieve the highest superposition between each centroid of the pharmacophoric elements and a corresponding local minimum of the MIFs. Such a procedure yielded a unique alignment for each pharmacophore so that 12 ligand−protein complexes could be modeled on the basis of four reference compounds with the purpose of refining the receptor model. Each complex was in fact relaxed (according to a protocol fully described in this report) and evaluated in terms of energies and "feature correspondence" to pick both

Table 2. Cost, Statistical Parameters, and Composition Features Associated with the First 10 Pharmacophoric Hypotheses Generated by Catalyst

| Hypo | cost[a] | statistical parameter | | | composition feature[b] | | | | |
		rmsd	r^2_{tr-set}	$r^2_{test-set}$	1	2	3	4	5
1	163.3	1.05	0.933	0.744	Hyd	Hyd	Hyd	RA	PI
2	167.8	1.17	0.917	0.806	Hyd	Hyd	Hyd	HBA	PI
3	168.7	1.18	0.915	0.839	Hyd	Hyd	Hyd	HBA	HBA
4	170.4	1.22	0.909	0.854	Hyd	Hyd	Hyd	RA	HBA
5	172.1	1.26	0.903	0.827	Hyd	Hyd	Hyd	RA	HBA
6	174.0	1.28	0.900	0.852	Hyd	Hyd	Hyd	HBA	HBA
7	174.9	1.31	0.895	0.738	Hyd	Hyd	Hyd	RA	HBA
8	175.0	1.30	0.897	0.840	Hyd	Hyd	Hyd	HBA	HBA
9	175.2	1.31	0.895	0.809	Hyd	Hyd	Hyd	HBA	HBA
10	175.6	1.32	0.893	0.760	Hyd	Hyd	Hyd	RA	HBA

[a] All costs are reported in bits. Fixed cost = 155.3 is the cost of a theoretical ideal hypothesis that is able to perfectly predict activities. Null cost = 290.8 is the cost of a hypothesis that gives no correlation between experimental and predicted activities. [b] Hyd: hydrophobic. RA: ring aromatic. PI: positive ionizable. HBA: hydrogen bond acceptor.

the optimum hA$_3$AR model and the best performing pharmacophore out of the three options investigated.

The selected pharmacophore was used afterward to export the relative alignment of four further compounds. The predictive power of the ligand−receptor model chosen was finally established by finding a quantitative correlation between experimental and theoretical values of free energies of binding, calculated by the application of a scoring function.

Finally, some novel putative A$_3$ antagonists were designed, synthesized, and biologically evaluated to test the reliability of our combined modeling strategy.

Results and Discussion

Pharmacophore Generation. hA$_3$AR antagonists are characterized by great structural diversity, making it difficult to find a common chemical pattern.[9−21,31] Nevertheless, certain common electronic and steric features have already been reported in the literature based on a combination of ab initio calculations, electrostatic potential map comparison, and steric and electrostatic alignment (SEAL) analyses.[31] In this study we exploited the ability of the Catalyst 4.6 software package[32] to find a common alignment for a comprehensive set of 55 A$_3$ antagonists (see Table 1) with the aim of explaining most of their structure−activity relationships.

The entire set of compounds, with activity data spanning 5 orders of magnitude (from 10^{-2} to 10^3 nM), was divided into a training set of 38 compounds and a complementary test set of 17 compounds (see Table 1), following Catalyst's guidelines.[33] In particular, (i) derivative **1k** (the most potent and selective A$_3$ antagonist ever reported)[12] was included in the training set because the software pays particular attention to the most active compound while generating the chemical feature space and (ii) the types and relative positions of the chemical features (substitution patterns) shown by the molecules were maximized because the program recognizes the molecules as collections of chemical features, not as assemblies of atoms or bonds.

Ten hypotheses were collected during a first pharmacophore generation, whose details are reported in Table 2. The 12.3 bit cost range gained over the models suggested the existence of a strong signal generated by the training set; moreover, a difference greater than 100 bits between the cost of each hypothesis and the null cost was indicative of more than 90% of true correlation.[33]

A careful analysis was performed on the generated hypotheses with the aim of selecting the most significant ones for further
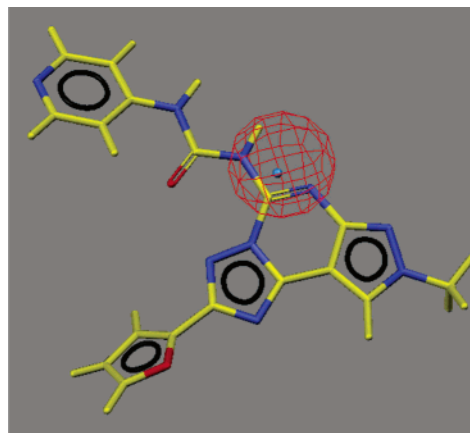
Figure 1. Compound **1k**. The red sphere shows the positive ionizable feature (PI) located in front of the guanidine moiety.

investigation. In the first place, the prediction of the test set ($r^2_{test-set}$) was used as the selection standard. To improve this rule, hypotheses were discarded, which estimated the activity of the most potent compound (**1k**) out of the correct 10^{-2} nM range. We believe indeed it was crucial that the activity of this compound was well estimated for a hypothesis to be considered reliable. Finally, the first two hypotheses of Table 2 were discarded, since they contained a doubtful positive ionizable feature (PI). A guanidine scaffold was recognized by Catalyst in several of our hA$_3$AR antagonists so that in a few hypotheses a centroid was located in an area between N^5, C5 and N6 of the pyrazolotriazolopyrimidine nucleus (see the case of compound **1k**, shown in Figure 1), indicating the presence of a potentially positively ionizable group. In short, the software was not able to discriminate between a guanidine system substituted with electron-withdrawing groups, which, as in our case, is not protonated at physiological pH, and a basic unsubstituted guanidine group (fairly protonated).

On the basis of such considerations, hypotheses 4 (HYPO1 in the following) and 6 (HYPO2 in the following) of Table 2 were chosen for further evaluation. HYPO1 and HYPO2 exhibited, respectively, correlation coefficients $r^2 = 0.909$ and $r^2 = 0.900$ for the training set and $r^2 = 0.854$ and $r^2 = 0.852$ for the test set. The activity of compound **1k** was well estimated by both HYPO1 ($K_{calc} = 5.6 \times 10^{-2}$ nM) and HYPO2 ($K_{calc} = 8.4 \times 10^{-2}$ nM). In Figure 2 the entire set of features of both pharmacophores is displayed superposed to this derivative. Both hypotheses were characterized by five features and shared a common scheme consisting of three hydrophobics at the vertexes of a triangle (HYD1, HYD2, and HYD3). They differed for a hydrogen bond acceptor (HBA1) pointing toward opposite directions and for a hydrogen bond acceptor (HBA2), which replaced, in HYPO2, the ring aromatic (RA) found in HYPO1.

Experimental and calculated (estimated or predicted by Catalyst) A$_3$ affinity values of all the compounds used in the computational studies are shown in Table 3, while the regression, based on HYPO1, of experimental versus estimated/predicted affinities is shown in Figure 3.

As shown in Table 3 with regard to HYPO1 and HYPO2, the ratio between calculated and experimentally measured K_i values of the compounds (error columns) was generally better than 10-fold and in most cases better than 3-fold. Taking into account this result and considering that the strong affinity values shown by **1k** might signify that it possesses all the crucial groups involved in ligand−receptor interactions, we could assume that both HYPO1 and HYPO2 accounted for relevant interactions between antagonists and hA$_3$AR. Furthermore, the soundness
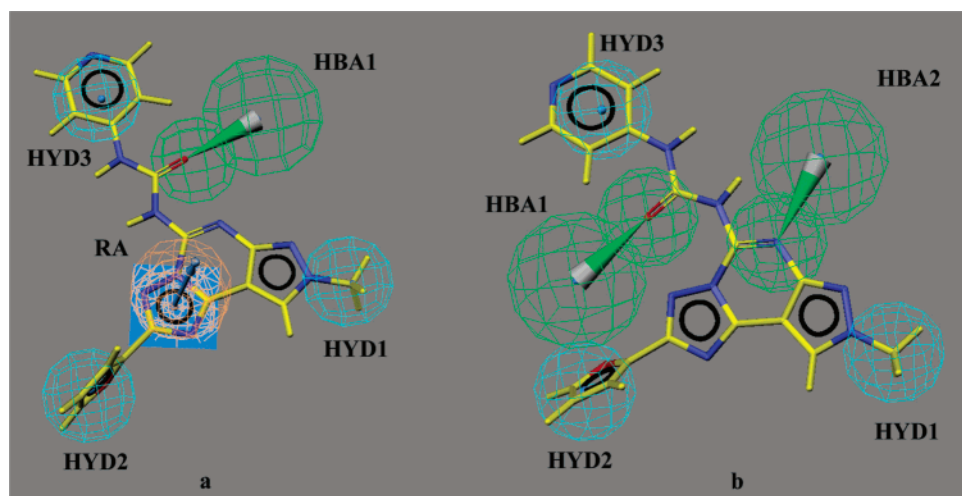
Figure 2. HYPO1 (a) and HYPO2 (b) superposed to compound **1k**. Pharmacophoric features are color-coded: sky blue for hydrophobic (HYD), green for hydrogen bond acceptor (HBA), and orange for aromatic ring (RA).
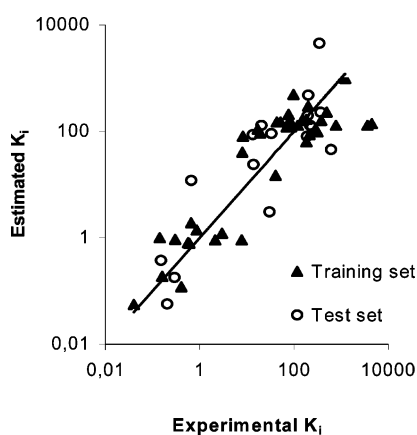

Figure 3. Regression of experimental versus estimated/predicted A_3 affinities (nM) based on HYPO1 (logarithmic scale), for each member of the training and test sets.

Figure 4. HYPO3 superposed to compound **1k**. Pharmacophoric features are color-coded: sky blue for hydrophobic (HYD), green for hydrogen bond acceptor (HBA), and magenta for hydrogen bond donor (HBD).

of both HYPO1 and HYPO2 hypotheses was supported by literature reports that stressed that a wide $\pi-\pi$ interaction involving the pyrazolotriazolopyrimidine system and the C2-furyl substituent might be crucial for A_3 antagonism,[31] while hydrophilic interactions are probably responsible for A_3 selectivity.

In any case, on the basis of what has been already reported by some of us about the importance of a hydrogen bonding donor (HBD) interaction between the NHCONH group present on most of the compounds considered in this study and hA_3-AR,[9,12] we then pushed Catalyst to generate new hypotheses with an HBD feature. Accordingly, we set up a possible adjustment to correct our computational protocol (see the Experimental Section for details). Catalyst's default spacing value (that is, the minimum distance between the location of actual features) was hypothesized to be the critical control parameter that had not worked properly for our set of compounds. As a result of this effort, 10 new HBD-endowed hypotheses were collected whose details are reported in Table 4, which presented similar statistical data with respect to the ones previously generated. Among those hypotheses possessing the HBD feature, the one ranked 9th (HYPO3 in the following) was chosen for further investigation according to the aforementioned selection rules.

In Figure 4 the entire set of features of HYPO3 is displayed superposed to compound **1k**. Once again, HYPO3 presented the recurring scheme of three hydrophobic interactions lying at
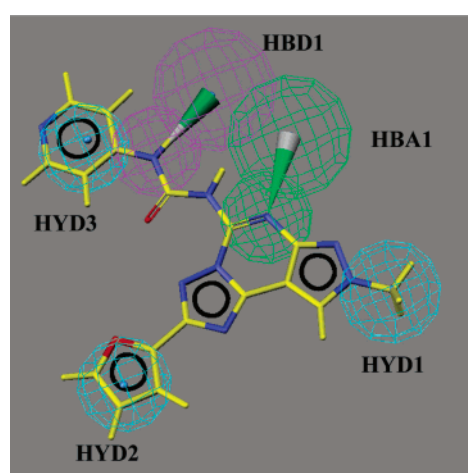
the vertexes of a triangle. No more RA features were present in the model, while two hydrophilic interactions (one HBA and one HBD) appeared at one side of the triangle. This hypothesis, like HYPO1 and HYPO2, was able to estimate/predict the activities of both training and test sets in a satisfactory manner (see Table 3), showing indeed a correlation coefficient $r^2 = 0.91$ for the training set and $r^2 = 0.87$ for the test set. Moreover, while two inactive compounds (**4a** and **1b**) were completely "mis-predicted" by HYPO3, most of the other compounds were fairly well-predicted with an error lower than ±3.

HYPO1, HYPO2, and HYPO3 were then exported and manually docked into the receptor model as described later in this article.

Receptor Modeling and Structure Optimization. All the information regarding the primary structure of the human A_3 receptor and the subdivision into transmembrane, cytoplasmatic, and extracellular domains was obtained from the GPCR Data Bank.[34] A raw structure of hA_3AR was obtained through molecular modeling, using bovine rhodopsin as a template.[30] The receptor−template superposition was carried out maintaining the maximum analogy between them and choosing the regions with a conserved or semiconserved sequence. The alignment was studied on several adenosine receptors by means of the ClustalW program[35] and was guided by the highly

Table 3. Experimental ($K_{i,exp}$) and Calculated ($K_{i,calcd}$) Affinity Values (nM) of All the Compounds Used in the 3D-QSAR Studies

		HYPO1		HYPO2		HYPO3	
compd	$K_{i,exp}$	$K_{i,calcd}$	error	$K_{i,calcd}$	error	$K_{i,calcd}$	error
1a	40	15	−2.6	8.4	−4.8	6.6	−6.0
1b	3600	130	−28.0	160	−22.0	160	−22.0
1c	0.4	0.12	−3.3	0.11	−3.5	0.092	−4.4
1d	0.14	1.0	7.2	0.46	3.3	0.41	2.9
1e	0.86	1.4	1.6	1.3	1.5	0.86	1.0
1f	0.56	0.81	1.4	1.6	2.8	0.49	−1.1
1g	0.3	0.93	3.1	0.65	2.2	0.58	1.9
1h	2.1	0.9	1.6	0.69	−3.0	0.67	−3.1
1i	0.16	0.19	1.2	0.14	−1.2	0.093	−1.7
1j	0.6	0.79	1.3	0.74	1.2	0.33	−1.8
1k	0.04	0.056	1.4	0.084	2.1	0.062	1.6
1l[a]	613	45	−13	96	−6.4	99	−6.2
1m[a]	0.29	0.18	−1.6	3.3	11	0.11	−2.7
1n[a]	348	4500	13.0	2800	7.9	3400	9.8
1o[a]	0.2	0.057	−3.5	0.17	−1.2	0.069	−2.9
1p[a]	0.65	12	19.0	7.1	11.0	6.3	9.7
1q[a]	0.15	0.38	2.5	0.57	3.8	0.17	1.1
1r[a]	30	3.1	−9.6	4.2	−7.1	2.6	−11.0
2o	85	120	1.4	240	2.9	200	2.3
2b	3	1.2	−2.5	1.1	−2.8	7.9	2.6
2c	0.65	1.9	2.9	1.7	2.6	5.7	8.7
2d	7.7	0.9	−8.6	0.61	−13.0	8.4	1.1
2e[a]	13.9	24	1.8	180	13.0	140	9.9
3a	17	110	6.2	180	11.0	170	9.9
3b	200	300	1.5	390	2	350	1.7
3c	96	500	5.2	310	3.3	210	2.2
3d	69	120	1.7	300	4.4	69	2.9
3e	310	98	−3.2	120	−2.7	130	−2.4
3f	770	130	−6	250	−3.1	190	−4
3g	150	160	1.1	160	1.1	150	1
3h	76	210	2.7	130	1.7	170	2.2
3i	1200	1000	−1.2	680	−1.7	960	−1.2
3j	490	230	−2.2	130	−3.8	180	−2.8
3k	51	150	2.9	120	2.3	150	2.9
3l	260	97	−2.7	94	−2.8	76	−3.5
3m	180	64	−2.8	52	−3.4	42	−4.3
3n	82	160	1.9	130	1.6	160	1.9
3o[a]	200	480	2.4	420	2.1	290	1.4
3p[a]	360	230	−1.5	280	−1.3	190	−1.9
3q[a]	240	120	−2	370	1.5	180	−1.3
4a	4500	140	−32.0	110	−40.0	100	−44.0
4b	210	86	−2.5	110	−2	110	−1.9
4c	180	170	−1.1	200	1.1	260	1.4
4d	43	150	3.6	170	3.9	150	3.4
4e	120	130	1.1	120	1.0	130	1.1
4f	8.3	81	9.8	100	12.0	100	12.0
4g	19	94	5.0	160	8.2	75	4.0
4h	7.9	40	5.0	19	2.4	16	2.0
4i[a]	20	130	6.5	130	6.5	100	5.2
4j[a]	33.3	91	2.7	100	3.1	110	3.3
4k[a]	194	200	1.1	130	−1.4	97	−2.0
4l[a]	188	80	−2.4	98	−1.9	86	−2.2
4m[a]	13.4	86	6.4	170	13	120	9.2
5a	380	160	−2.4	180	−2.1	140	−2.7
5b[a]	219	130	−1.7	140	−1.6	140	−1.6
16[b]	5.1	5.1	1.0	NC[c]	NC[c]	NC[c]	NC[c]
17[b]	2.0	5.4	2.7	NC[c]	NC[c]	NC[c]	NC[c]
18[b]	34	8.7	−3.9	NC[c]	NC[c]	NC[c]	NC[c]

[a] Compounds included in the test set. [b] New A_3 antagonist designed, synthesized and biologically evaluated, to test the reliability of the computational approach. [c] Not calculated.

conserved amino acid residues (see the Supporting Information), including the D/ERY motif (D/E3.49, R3.50, and Y3.51), the two Pro residues P4.50 and P6.50, and the NPXXY motif in the TM7 (N7.49, P7.50, and Y7.53).[36]

The homology model directly obtained using bovine rhodopsin as a template was not able to take into account all the mutagenesis data reported concerning antagonists of hA$_3$AR (see Table 5). In particular, in contrast with these data, Hys95 and Hys272 did not point toward the intrahelical channel. Therefore,

Table 4. Cost, Statistical Parameters, and Composition Features Associated with the Second 10 Pharmacophoric Hypotheses Generated by Catalyst

		statistical parameter			composition feature[b]				
Hypo	cost[a]	rmsd	r^2_{tr-set}	$r^2_{test-set}$	1	2	3	4	5
1	176.9	1.05	0.934	0.821	Hyd	Hyd	Hyd	Hyd	HBD
2	178.2	1.08	0.930	0.811	Hyd	Hyd	Hyd	Hyd	HBA
3	183.0	1.20	0.913	0.822	Hyd	Hyd	Hyd	HBD	RA
4	183.7	1.18	0.916	0.821	Hyd	Hyd	Hyd	HBA	HBA
5	184.7	1.23	0.908	0.800	Hyd	Hyd	Hyd	HBA	HBA
6	185.1	1.23	0.908	0.857	Hyd	Hyd	Hyd	HBA	HBD
7	185.2	1.24	0.906	0.743	Hyd	Hyd	Hyd	HBA	RA
8	185.2	1.21	0.912	0.795	Hyd	Hyd	Hyd	HBA	HBA
9	185.3	1.22	0.909	0.870	Hyd	Hyd	Hyd	HBA	HBD
10	186.1	1.17	0.918	0.738	Hyd	Hyd	Hyd	HBA	HBD

[a] All costs are reported in bits. Fixed cost = 155.34 is the cost of a theoretical ideal hypothesis that is able to perfectly predict activities. Null cost = 290.81 is the cost of a hypothesis that gives no correlation between experimental and predicted activities. [b] Hyd: hydrophobic. RA: ring aromatic. PI: positive ionizable. HBA: hydrogen bond acceptor.

Table 5. Mutational Analysis for the Human A_3 Receptor Antagonists Interaction

region	A_3AR	mutational results
TM3	H95	A: reduction of affinity[a]
L 4−5	K152	A: reduction of affinity[a]
TM6	W243	A: reduction of affinity[a]
	L244	A: modest variation[a]
	S247	A: modest reduction of affinity[a]
	N250	A: loss of binding[a]
TM7	H272	E: reduction of affinity[a]
	Y282	F: reduction of affinity[b]

[a] See ref 40. [b] See ref 39.

the TM3 and TM7 had to be rotated respectively by 60° clockwise and 90° counterclockwise (extracellular point of view) to let them turn toward the intrahelical channel, thereby allowing the interaction of Hys95 and Hys272 with the ligands. On the other hand, in agreement with the findings of Gouldson et al.,[37] rotations and translations of the transmembrane (TM) domains are important steps in a ligand−receptor interaction process in different GPCRs. Because of the antagonist profile of the ligands considered, possible rearrangements of the receptor in an activated form able to interact with agonists were not taken into account. The hA$_3$AR model so obtained was optimized through the procedure fully described in the Experimental Section, and the seven helices were then disassembled.

Individual molecular interaction fields (MIFs) were calculated for every transmembrane helix by means of the GRID program[38] with the aim of determining energetically favorable interaction sites on each one of them. Several probes were used at this stage (see Table 6 for details) to investigate the ligand−receptor binding mode.

After the seven helices were reassembled, the receptor was displayed together with the points of local minimum energy of the MIFs located at their proper position in 3D space. At this point, Catalyst hypotheses were manually docked one by one, coupling this operation with a manual rearrangement of the relative positions and orientations of the helices in order to (a) superpose each pharmacophoric feature found by Catalyst on a minimum of the corresponding MIF (see Table 6) and (b) retain the crucial interactions between the pharmacophore features and the most important residues, as highlighted by site directed mutagenesis studies.[39−42]

In this manner, three models of the receptor−antagonist complex were obtained (MODEL1, MODEL2, MODEL3) that differed from each other for the binding mode of the ligands as
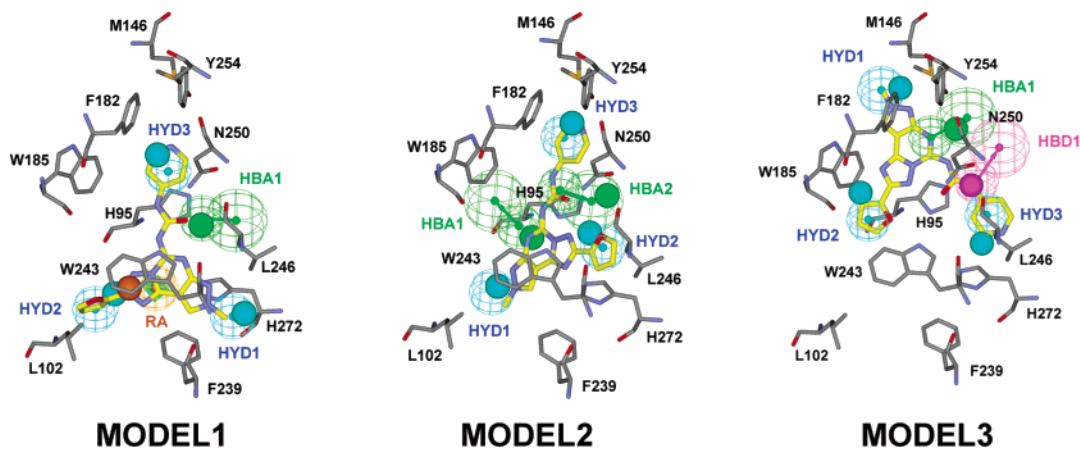
Figure 5. From left to right, the three receptor complexes of hA$_3$AR with **1k** (MODEL1, MODEL2, and MODEL3) are shown, each one superposed on the alignment between the complementary pharmacophoric hypothesis and the MIFs (displayed as spheres). In sky-blue the minima obtained with the DRY probes are represented. In green are those calculated with O and N:= probes. In orange are those derived from the calculation with the C1= probe, and in magenta is the one obtained with the NH= probe.

Table 6. Details of the Probes Used for MIF Calculations[a]

probe	brief description	corresponding catalyst feature
H	hydrogen	HYD
DRY	hydrophobic probe	HYD, RA
C1=	sp^2 CH aromatic or vinyl	RA
N:=	sp^2 N with lone pair	HBA
N1=	sp^2 amine NH cation	PI, HBD
NH=	sp^2 NH with lone pair	HBA, HBD
N1+	sp^3 amine NH cation	PI, HBD
N1:	sp^3 NH with lone pair	HBA, HBD
N2	neutral flat NH$_2$, e.g., amide	HBD
N2=	sp^2 amine NH$_2$ cation	PI, HBD
N2+	sp^3 amine NH$_2$ cation	PI, HBD
N2:	sp^3 NH$_2$ with lone pair	HBA, HBD
NM3	trimethylammonium cation	PI
O1	alkylhydroxyl OH group	HBA, HBD
OC2	ether or furan oxygen	HBA
O	sp^2 carbonyl oxygen	HBA

[a] The corresponding catalyst features are reported in the last column.

defined by the three pharmacophoric hypotheses (HYPO1, HYPO2, and HYPO3).

To determine which of the three models was the most reliable one, derivatives **1j**, **1k**, **2c**, and **3a** were chosen among those used in the 3D-QSAR studies and manually docked into the receptor, using the three alignment rules and conformations defined by the corresponding pharmacophoric hypotheses.

Figure 5 shows the three models (compound **1k** is displayed as reference) together with the alignments between selected local minima of the MIFs (calculated as described above) and the three pharmacophoric hypotheses HYPO1, HYPO2, and HYPO3.

In MODEL1, the aromatic ring feature RA (matched by the core of **1k**) resulted in being superimposed on one of the C1= probe minima, highlighting a $\pi-\pi$ interaction with Trp243. In fact, this residue has been widely reported as playing an important role in antagonist recognition.[40−42] HBA1 mapped profitably an O probe minimum, digging up a possible hydrogen bond between the C=O of the ligand and the side chain NH of Asn250. Notably, the mutation of this residue causes loss of affinity for both agonists and antagonists.[40−42] Finally, HYD1, HYD2, and HYD3 resulted in being superimposed on three DRY minima and were accommodated into three receptor hydrophobic clefts (H1, H2, and H3) delimited, respectively, by (i) Phe239, Trp243, Hys272; (ii) Leu102, Phe239, Trp243; and (iii) Hys95, Phe182, Trp185, Tyr254.

In MODEL2, the overlap between HBA1 and the O probe minimum as well as the correspondence between HYD3 and the lipophilic cleft H3 were maintained. However, different from MODEL1, HYD1 corresponded to the lipophilic cleft H2 while HYD2 corresponded to a lipophilic interaction with Leu246, close to the cleft H1. Regarding HBA2, this feature (not present in HYPO 1) was found to overlap an N:= probe minimum, suggesting a possible hydrogen bonding interaction between **1k** (N6 of the aromatic core) and the backbone NH of His95.

Finally, the features of HYPO3 determined a completely different disposition of the pharmacophore inside MODEL3 (see Figure 5): HYD1 was accommodated into a lipophilic cleft delimited by Met146, Phe182, and Trp185 (roughly corresponding to the H3 cleft); HYD3 matched a DRY minimum next to Leu246 and His272; HYD2 corresponded to an energy-favorable lipophilic interaction with Trp185. Regarding electrostatic interactions, HBA1 corresponded to an H-bond with Tyr254 and HBD1 matched an H-bond between the C=O of Asn250 and the NH of **1k**.

The 12 generated complexes (obtained from the docking of **1j**, **1k**, **2c**, and **3a** into the three MODELs) were then subjected to a relaxation protocol (see Experimental Section).

In MODEL1 all four ligands established the expected interactions with His95, Trp243, His272 and formed one H-bond with Asn250.

In MODEL2 the lipophilic interactions with His95, Trp243, and His272 were detected for all four ligands, while only three ligands out of the four (**1j**, **1k**, and **2c**) possessed the crucial hydrogen bond with Asn250 (see Table 6). Furthermore, none of the complexes showed the hydrogen bond predicted by HYPO2 between the N6 nitrogen of the aromatic core and the backbone NH of His95 (HBA2 feature).

In MODEL3 all the ligands interacted with His95, Trp243, His272, and Asn250; however, as a result of the optimization procedure, both compounds **2c** and **3a** acted as a hydrogen bond acceptor with respect to Asn250, in contrast to the pharmacophoric hypothesis (HYPO3) which predicted an HBD feature (HBD1).

Therefore, although mutagenesis data were generally verified for all three models, only MODEL1 was able to fulfill both mutagenesis data and the Catalyst predicted pharmacophoric framework for all the compounds tested.

The interaction energies of all 12 complexes were then calculated by subtracting the energy of the separate ligand and receptor from the energy of the receptor−ligand complex, and

Table 7. Interaction Energies of Compounds **1i**, **1k**, **2c**, and **3a** in the Three Considered Alignment Models: MODEL1, MODEL2, and MODEL3

compd	interaction energies (kJ/mol)		
	MODEL 1	MODEL 2	MODEL 3
1j	−55.9	−52.1	−53.5
1k	−61.4	−53.4	−56.8
2c	−58.5	−53.5	−55.7
3a	−55.2	−47.0	−47.6

Table 8. A_3 Affinity (K_i), Experimental Binding Free Energy (G_{exptl}), and AutoDock Binding Free Energy (G_{calcd}) into the Three Models of Compounds **1k**, **1j**, **2c**, **2d**, **3a**, **3i**, **4a**, and **4h**

compd	K_i (nM)	G_{exptl} (kcal/mol)	G_{calcd} (kcal/mol)		
			MOD 1	MOD 2	MOD 3
1k	0.04	−14.18	−12.05	−11.10	−11.29
1j	0.60	−12.57	−12.84	−12.79	−11.00
2c	0.65	−12.53	−12.80	−12.09	−11.64
2d	7.66	−11.07	−10.81	−9.30	−9.46
3a	17	−10.59	−11.78	−9.58	−11.24
3i	1180	−8.08	−9.22	−7.72	−10.03
4a	4470	−7.29	−10.00	−9.00	−7.71
4h	7.94	−11.04	−10.54	−8.57	−11.42

the values calculated are reported in Table 7. Generally it was not possible to find a quantitative correlation between calculated values and affinities of the compounds mainly because of the lack of the solvation and entropic terms. However, in this case, only the interaction of the same ligand, though in different orientations, in the same receptor was to be evaluated, and therefore, the solvation and entropic contributions could be considered approximately constant. As shown in Table 7, MODEL1 yielded the highest interaction energy values for all four ligands. Although the difference in energies among the three models was small and probable within the error of the method, the fact that the best interaction energy for all ligands was found with MODEL1 strengthens the hypothesis that this model could be considered the most reliable one.

In a third check, an assessment of the predictive power of the three models was carried out. The free energies of binding of the complexes with several compounds were calculated by means of the AutoDock 3.0 scoring function.[43] This docking application proved in fact to be reliable in many studies present in the literature,[44−46] since its free energy function, based on the principles of QSAR, has been parametrized using a large number of protein−inhibitor complexes for which both structure and inhibition constants were known. Accordingly, compounds **2d**, **3i**, **4a**, and **4h** were docked in turn, applying the protocol already discussed for compounds **1j**, **1k**, **2c**, and **3a**.

As shown in Table 8 and Figure 6, a reasonable quadratic correlation between experimental and calculated values of free energy of binding was found for MODEL1 ($r^2 = 0.69$). In contrast, a weaker free energy correlation was obtained for MODEL2 and MODEL3 (values of 0.56 and 0.57, respectively). All these results suggested MODEL1 as the most reliable one, and for this reason it was selected for further analysis.

With the aim of achieving a qualitative knowledge of the features of hA$_3$AR, the eight relaxed complexes of compounds **1k**, **1j**, **2c**, **2d**, **3a**, **3i**, **4a**, and **4h** were compared among each other through the superposition of the seven helices. The outcome of such a procedure is shown in Figure 7. The most evident result was that the receptor model was able to vary the width and shape of its three hydrophobic clefts in order to accommodate different ligands. In particular, Trp185 could act as a gate, making the H2 and H3 clefts wider or narrower. In the case of compounds showing $K_i < 1$ nM (left part of Figure
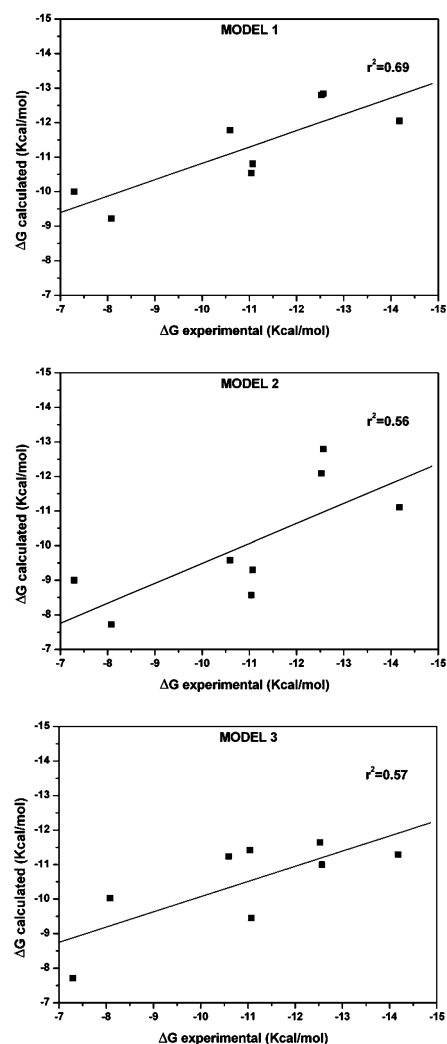
Figure 6. Experimental versus calculated (AutoDock) binding energy of compounds **1k**, **1j**, **2c**, **2d**, **3a**, **3i**, **4a**, and **4h**.
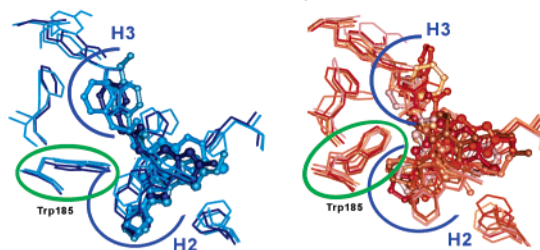
Figure 7. Superposition of the complexes of hA$_3$AR with the most active ligands **1j**, **1k**, and **2c** (left) and with the less active ones **2d**, **3a**, **3i**, **4a**, and **4h** (right). For sake of clarity, only residues under consideration are reported.

7), H2 was very small, thus allowing a perfect matching with the ligand, while the wider H3 was able to accommodate long chains such as phenylcarbamoyl moieties. On the other hand, for compounds showing $K_i > 1$ nM (right part of Figure 7), Trp185 was in an "open" conformation so that weaker contacts were possible with the ligands. Therefore, the model seemed to be able to discriminate between very active compounds ($K_i < 1$ nM) and less active ones ($K_i > 1$ nM).

Regarding the interactions between **1k** and the hA$_3$ receptor, beyond the above-mentioned interactions and already suggested by site directed mutagenesis studies, residue Tyr254 also played an important role in our A$_3$ model because it formed an H-bond with the pyridyl ring of the ligand (see Figure 8). This interaction
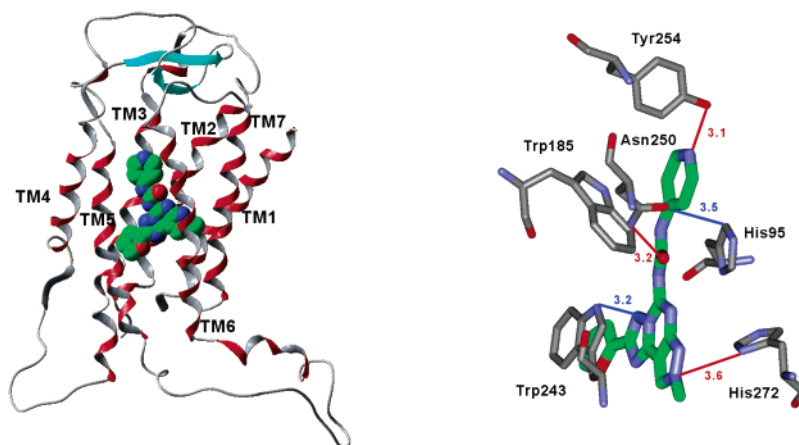
Figure 8. Side view of hA₃AR complexing **1k** into its intrahelical region (MODEL1, left) and details of relevant binding interactions (right).

could justify the improved activity of compounds such as **1k**, presenting a proper hydrogen-bonding acceptor group in that region (4-pyridyl) and the irreversible inhibition by *p*-fluoro-sulfonylpyrazolo[4,3-*e*]-1,2,4-triazolo[1,5-*c*]pyrimidine derivatives.[47] Furthermore, because of the fact that Tyr254 is a nonconserved residue in other adenosine receptors, this interaction could also explain the high selectivity shown by **1k**.

Design and Synthesis of hA₃AR Antagonists. The analysis of the recognition geometry of compound **1k** in MODEL1 suggested some structural changes to be made on the pyrazolotriazolopyrimidines, with the aim of improving their water solubility and ADME properties as well as the activity/selectivity profile. In particular, a small hydrophilic pocket bordered by two serine residues (Ser242 and Ser275) lay empty near the H1 cleft of the receptor. Hence, the introduction of a short alkyl chain at N⁸ of **1k**, terminating with a hydrophilic group, was hypothesized to verify the possibility of binding interactions within this pocket.

In contrast, it appears that the interactions with His98, Trp243, Asn250, Tyr254, and His272 (see Figure 8) are to be conserved; therefore, the tricyclic system of **1k** together with the pyridine–urea moiety should be maintained.

Compounds **16**−**18** (Scheme 2) to be proposed for the synthesis were then designed and virtually evaluated in silico (applying the whole modeling procedure described above).

The synthesis of compounds **16**−**18** was performed using the synthetic strategy depicted in Schemes 1 and 2. Alkylation of the 2-(furan-2-yl)-7*H*-pyrazolo[4,3-*e*]-1,2,4-triazolo[1,5-*c*]pyrimidin-5-ylamine **6**[10,48] with 2-iodoethanol or benzyl-3-bromopropyl ether in DMF and 60% NaH afforded compounds **7**[48] and **8**, which were separated from the corresponding N⁷ isomers by flash chromatography.

The free hydroxylic group of the N⁸ isomer of compound **7** was then protected by reaction with benzyl bromide to furnish derivative **9**[48] (Scheme 1). As reported in Scheme 2, the free amino group at the 5 position of compounds **8** and **9** was converted into the corresponding ureas **13**−**15** by treatment with freshly prepared 3- or 4-pyridyl isocyanates **12a** or **12b**, respectively. The preparation of the intermediates **12a,b** is described in the literature[48−50] and illustrated in Scheme 2. The commercially available nicotinoyl and isonicotinoyl hydrazides (**10a** and **10b**) were converted into the corresponding acyl azides (**11a** and **11b**) by reaction with sodium nitrite and aqueous HCl. The azides were then converted into the isocyanates **12a** and **12b** by Curtius rearrangement induced by heating the azides in dry toluene for 2 h. The crude isocyanates obtained were added to the tricyclic compounds **8** and **9** dissolved in dry THF, and

Scheme 1[a]
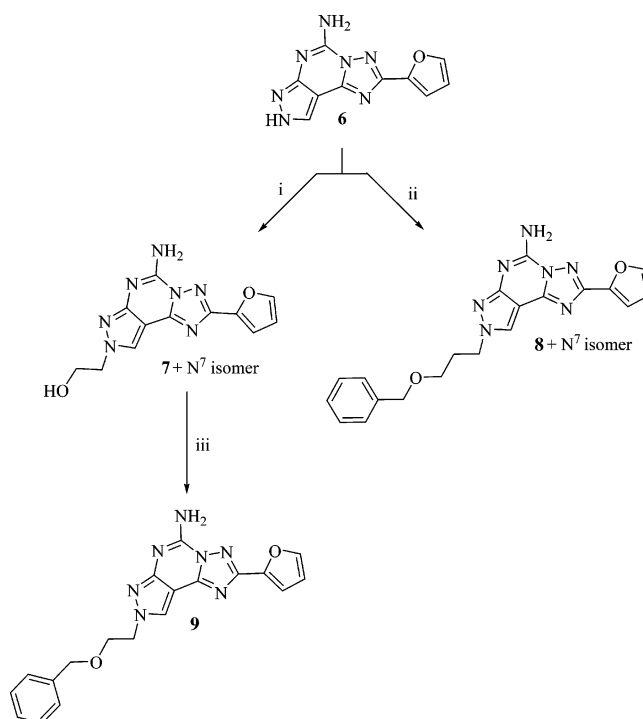
[a] Reagents: (i) 2-iodoethanol, 60% NaH, room temp; (ii) benzyl 3-bromopropyl ether, 60% NaH, 100 °C, 12 h; (iii) benzyl bromide, 60% NaH, room temp, 5 h.

the mixture was then refluxed for 5−8 h to afford compounds **13**−**15**. The final products **16**−**18** were achieved by deprotecting the ether function by treatment with HCO₂NH₄ and 10% Pd/C in dry acetone at reflux.

Compounds **13**−**18** were tested for their affinity toward human A₁, A₂A, A₂B, and A₃ adenosine receptors (see Experimental Section). The values measured for compounds **16**−**18** are shown in Table 9, to be compared with the theoretical values predicted for the A₃ receptor by both the AutoDock scoring function (notably, the scoring function hypothesized an activity between 0.5 and 2 nM for these ligands) and Catalyst (Table 3).

Compound **17** resulted in being the most promising selective A₃ antagonist. The docking of this derivative into MODEL 1 is shown in Figure 9. The expected hydrogen-bonding interaction between the hydroxyl substituent at N8 and Ser275 is highlighted. Even if the affinity of **17** for the A₃ receptor dropped about 2 orders of magnitude with respect to compound **1k**, its

Scheme 2[a]
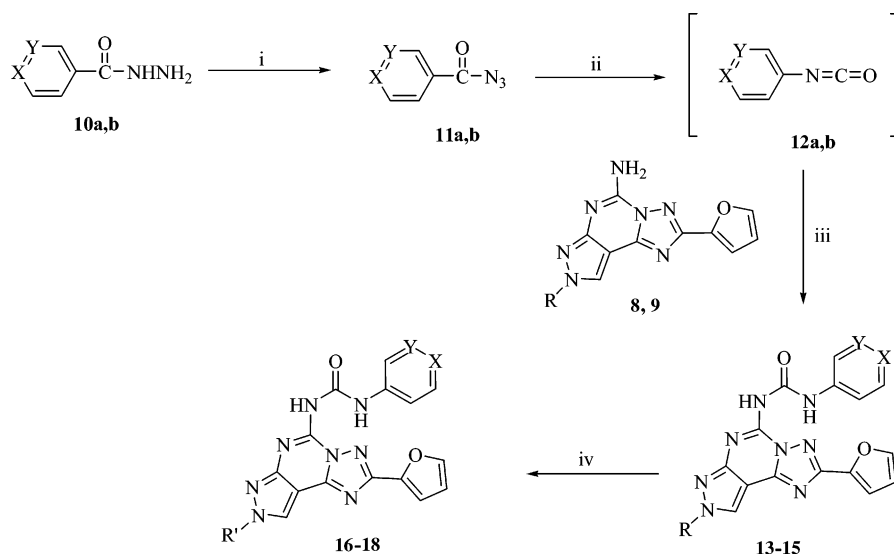
[a] Reagents: (i) NaNO$_2$, aqueous HCl, 0 °C, 1 h; (ii) toluene, 80 °C, 2 h; (iii) THF, reflux 5−8 h; (iv) acetone, HCO$_2$NH$_4$, 10% Pd/C, reflux 12 h. **10a**, **11a**, **12a**: X = CH, Y = N. **10b**, **11b**, **12b**: X = N, Y = CH. **13**: X = N, Y = CH, R = 2-benzyloxyethyl. **14**: X = N, Y = CH, R = 3-benzyloxypropyl. **15**: X = CH, Y = N, R = 2-benzyloxyethyl. **16**: X = N, Y = CH, R′ = 2-hydroxyethyl. **17**: X = N, Y = CH, R′ = 3-hydroxypropyl. **18**: X = CH, Y = N, R′ = 2-hydroxyethyl.

Table 9. Affinity Values of Compounds **16−18**

compd	K_i (nM)				
	hA$_1$[a]	hA$_{2A}$[b]	hA$_{2B}$[c]	hA$_3$[d]	predicted hA$_3$[e]
16	>1000	>1000	>1000	5.1 (4.1−6.5)	1.78
	(74%)	(96%)	(71%)		
17	350 ± 30	>1000	>1000	2.0 (1.7−2.4)	0.78
		(95%)	(73%)		
18	>1000	>1000	>1000	34 (28−40)	1.58
	(92%)	(93%)	(99%)		

[a] Displacement of specific [^{3}H]DPCPX binding at human A$_1$ receptors expressed in CHO cells. [b] Displacement of specific [^{3}H]ZM 241385 binding at human A$_{2A}$ receptors expressed in CHO cells. [c] Displacement of specific [^{3}H]MRE 2029F20 binding at human A$_{2B}$ receptors expressed in CHO cells. [d] Displacement of specific [^{3}H]MRE 3008F20 binding at human A$_3$ receptors expressed in CHO cells. [e] Predicted A$_3$ K_i affinity (using our A$_3$ model and AutoDock scoring function).
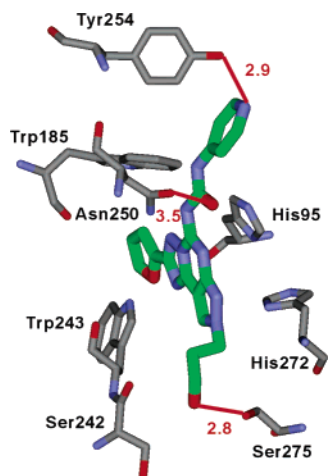

Figure 9. Compound **17** docked into the putative binding site.

receptor subtype selectivity was completely conserved, and this could confirm the importance of the pyridine ring for the A$_3$ selectivity. As regards the affinity drop, this could be due to partial damage of the $\pi-\pi$ stacking interaction with Trp243 due to the formation of the new hydrogen bond (see Figure 9)

as well as to an entropy penalty associated with the high number of degrees of freedom of the alkyl chain. In any case, there is quite a good affinity prediction by our hA$_3$AR model.

Conclusions

In the research reported here we performed a pharmacophoric study using the software Catalyst, which yielded three different common feature hypotheses for antagonists of the human A$_3$ receptor. The statistical parameters of the three models, i.e., high cost differences with respect to null costs, suggested a possible reliability of all of them; moreover, they all showed the ability to predict affinity data for a test set of compounds, in good agreement with experimental data. The three pharmacophores referred to a recurring scheme consisting of three hydrophobic interactions lying at the vertexes of a triangle. They seemed particularly good in handling pyrazolotriazolopyrimidine derivatives, the most potent class of A$_3$ antagonists ever reported. On the other hand, our ligand based approach alone did not converge on a unique model and only the use of molecular modeling techniques allowed us to choose the most reliable pharmacophore.

The construction of a human G-protein-coupled receptor model through a homology procedure solely based on the bovine rhodopsin structure is quite an unreliable task because of usually low homology percentages and the high degree of mobility of the helices.[37] The use of mutagenesis data is nowadays an important improvement in the procedure because it allows us to take into account residues experimentally found to be necessary for interaction. The relative positions of these residues, however, remain unknown and can only be hypothesized through the docking into the receptor of a ligand, which retains all these interactions. Generally the alignment for this docking is to be manually performed. Differently, in the procedure described herein the use of a pharmacophoric model representing the activity data of a lot of ligands allowed the building of a receptor model in which the relative positions and distances between important residues were determined by the distances between pharmacophoric features.

As a whole, our combined modeling strategy slightly differed from canonical procedures. The building of 3D-QSAR models,

in fact, helped us to exploit a set of active molecules to highlight statistically relevant features in ligand−receptor interactions, and such information was crucial for generating a reliable model of hA₃AR when interacting with antagonists (MODEL1). The information produced through docking studies, in turn, allowed us to select the best performing pharmacophore model (HYPO1) among a set of plausible hypotheses.

MODEL1 seemed to be able to explain different modes of binding of very active compounds with respect to less active ones and also to reproduce free energies of binding with good approximation. The model was also able to explain the selectivity of **1k** toward hA₃AR due to the presence of the nonconserved residue Tyr254 and therefore suggested that a mutagenesis study on this residue could be of great importance to find out the molecular features determining the selectivity at the AR subtypes.

The reliability of our synergistic approach was tested by the rational design and synthesis of a series of novel compounds. Biological assays indicated that reasonably good activity values were reached and, at the same time, water solubility was enhanced compared to results of previously synthesized compounds.

Experimental Section

Pharmacophore Generation. The literature was searched for compounds showing the widest array of chemical features and the most homogeneous biological data.[9−21,31] Fifty-five compounds (see Table 1) with activity data spanning over 5 orders of magnitude (from 10^{-2} to 10^3 nM) were selected and divided into a training set (38 compounds) and a complementary test set (17 compounds). Biological data for all the inhibitors were reported as K_i.

Each compound was built using the 2D-3D sketcher implemented in Catalyst and then submitted to a conformational search. The "best conformer generation" method, which makes use of the Poling algorithm to reduce conformational redundancies, ensuring good space coverage,[51] was preferred and we found up to 250 conformers within 20.0 kcal/mol above the global minimum.

Because of the presence of great chemical functionalization in all compounds, the generator was constrained to generate sets of hypotheses bearing at least the following five features: hydrophobic (HYD), hydrogen bond acceptor (HBA), hydrogen bond donor (HBD), ring aromatic (RA), and positively ionizable atom (PI).

All compounds (each one with its conformational model) were put into a spreadsheet and associated with their affinity constants with the default uncertainty of 3. Because of the fact that the most active compound (**1k**) was the only one showing a K_i in the 10^{-2} nM range, the set of "active molecules" used by the software in the very first part of the calculation to generate hypotheses was reduced by diminishing from 3 to 2 the uncertainty parameter associated with **1k**. Otherwise, the software might have attached more statistical importance to ligands presenting lower affinity values just because many compounds carry a greater amount of information than a single one does.[33]

During the second generation of hypotheses, two more control parameters were changed from their default value; the MinFeatDist value was decreased from 300 to 100 (1 Å), and the Variable Tolerance value was set at 1. The first adjustment allowed the generator to retrieve hypotheses with a minimum interfeature distance down to 1 Å, while the second change allowed the tolerance of each feature to vary during generation to avoid overlap between features.

Molecular Modeling. Molecular mechanics (MM) and molecular dynamics (MD) calculations were performed using the AMBER force field[52] as implemented in the MacroModel software package,[53] using a "distance-dependent" dielectric constant of 4.0. Electrostatic charges for the set of ligands were calculated with the RHF/AM1 semiempirical calculation and RESP program.[54]

All MM minimizations were performed with either Polak−Ribier conjugate gradient or steepest descent as minimizers and with a threshold value of 0.05 kJ/(Å·mol) as the convergence criterion. The temperature was set at 300 K, and the time step was 1.0 fs in MD simulations.

All graphical manipulations and visualizations were performed by means of the InsightII,[55] UCSF-CHIMERA,[56] and WebLab Viewer[57] programs.

The alignment of several adenosine receptors was studied with the ClustalW program using the Blosum algorithm, with a gap open penalty of 10 and a gap extension penalty of 0.05. From the ClustalW alignment, the structure of the seven-TM helices of hA₃-AR and the first intracellular loop were constructed directly from the coordinates of the corresponding amino acids in rhodopsin by means of the Modeller program.[58] Through Maestro interface, the TM3 and TM7 were rotated respectively 60° clockwise and 90° counterclockwise (extracellular point of view) to let Hys95 and Hys272 turn toward the intrahelical channel. Because the amino acid length differs from the template and for the rotation of TM3 and TM7, the other loops were constructed by means of the "loop optimization method" of Modeller, applying the "very_slow" loop refinement method. The model was subjected to a preliminary minimization and to 400 ps of MD (after 50 ps of equilibration). The final structure was then minimized. When MD simulations were carried out in the gas phase, all the α carbons of the TM of the protein were blocked by means of decreasing force constants to simulate the stabilizing presence of the membrane around the receptor. For the first 200 ps, restraints with a force constant of 10 kcal/(mol·Å²) were applied to Cα, and for the remaining 200 ps these restraints were gradually reduced to 1 kcal/(mol·Å²).

The refinement of the ligand−protein complexes was initially performed by means of a total of 400 ps of MD. All the α carbons of the TMs and the main ligand−receptor interactions were constrained during the trajectory by decreasing the force constants. In detail, an initial restraint with a force constant of 10 kcal/(mol· Å²) was applied on the α carbons. This force constant decreased during the entire MD, and in the last 200 ps a value of 0.1 kcal/ (mol·Å²) was applied. As regards the H bond ligand−receptor interactions, suggested by the HBA1, HBA2, and HBD1 features found by Catalyst, a restraint of 50 kcal/(mol·Å²) was applied in order to stabilize ligand−receptor complex structures maintaining all these interactions. At the end of the MD simulation, three steps of minimization were applied on the average structure obtained during the last 100 ps of the MD run. During these three steps a restraint of 0.1 kcal/(mol·Å²) was applied on the α carbons, while with regard to the main ligand−receptor interactions, in the first two steps a restraint of 25 and 10 kcal/(mol·Å²) was applied and in the last one the restraints were removed.

The quantitative evaluation of the free energy of binding of the 12 complexes was performed by means of the AutoDock scoring function,[43] using the Lamarckian genetic algorithm. The region of interest used by AutoDock was defined considering compound **1k** docked in hA₃AR as a center group. In particular, a grid of 40, 54, and 50 points in the *x*, *y*, and *z* directions was built centered on the center of mass of **1k**. A grid spacing of 0.375 Å and a distance-dependent function of the dielectric constant were used for the calculation of the energetic maps.

General Chemistry. Reaction courses and product mixtures were routinely monitored by thin-layer chromatography (TLC) on silica gel (precoated F₂₅₄ Merck plates) and visualized with aqueous potassium permanganate or ethanolic ninhydrin solutions. Infrared spectra (IR) were measured on a Perkin-Elmer 257 instrument. ¹H NMR were determined in CDCl₃ or DMSO-d_6 solutions with a Bruker AC 200 spectrometer. Peak positions are given in parts per million (δ) downfield from tetramethylsilane as internal standard, and *J* values are given in Hz. Light petroleum refers to the fractions boiling at 40−60 °C. Melting points were determined on a Buchi− Tottoli instrument and are uncorrected. Chromatography was performed with Merck 60−200 mesh silica gel. All products reported showed ¹H NMR spectra in agreement with the assigned structures. Organic solutions were dried over anhydrous sodium

sulfate. Elemental analyses were performed by the microanalytical laboratory of Dipartimento di Chimica, University of Ferrara and were within ±0.4% of the theoretical values for C, H, and N.

Syntheses. 8-(3-Benzyloxypropyl)-2-(furan-2-yl)-8*H*-pyrazolo-[4,3-*e*]-1,2,4-triazolo[1,5-*c*]pyrimidin-5-ylamine (8). To a solution of **6** (0.6 g, 2.4 mmol) in dry DMF (10 mL) was added 60% NaH (0.12 g, 1 mol equiv), and the suspension was stirred at 0 °C for 10 min. Benzyl 3-bromopropyl ether (0.42 mL, 1 mol equiv) was added in small portions, and the mixture was heated at 100 °C for 12 h. The solvent was removed at reduced pressure, and the residue was dissolved in water (100 mL) and extracted with EtOAc (3 × 30 mL). The organic layer was dried (Na_2SO_4) and evaporated under vacuum. The residue obtained was purified by chromatography (EtOAc, 100%) to afford the N^8 isomer **8** as pale-yellow solid (0.36 g, 77%): mp 173−5 °C; ^{1}H NMR (CDCl$_3$) δ 2.24 (m, 2H), 3.49 (t, 2H, $J = 6.1$), 4.45 (s, 2H), 4.52 (t, 2H, $J = 6.2$), 5.97 (bs, 2H), 6.58 (m, 1H), 7.30 (m, 6H), 7.61 (m, 1H), 8.17 (s, 1H). Anal. ($C_{20}H_{19}N_7O_2$) C, H, N.

General Procedure for 5-[[(3(4)-Pyridyl)amino]carbonyl]-amino-8-(2-benzyloxyethyl)-2-(furan-2-yl)-8*H*-pyrazolo[4,3-*e*]-1,2,4-triazolo[1,5-*c*]pyrimidines (13 and 15). Amino compound **9**[48] (0.2 g, 5.3 mmol) was dissolved in dry THF (10 mL), and the freshly prepared 3(4)-pyridyl isocyanates[49,50,59] **12a,b** (5 mol equiv) were added. The mixture was refluxed under argon for 5−8 h. Then the solvent was removed under reduced pressure and the residue was purified by flash chromatography (EtOAc/MeOH, 8:2) to afford compounds **13** and **15** as solids.

5-[[(4-Pyridyl)amino]carbonyl]amino-8-(3-benzyloxypropyl)-2-(furan-2-yl)-8*H*-pyrazolo[4,3-*e*]-1,2,4-triazolo[1,5-*c*]pyrimidine (14). Amino compound **8** (0.18 g, 4.6 mmol) was dissolved in dry THF (10 mL), and the freshly prepared 4-pyridyl isocyanate[49,50,59] **12b** (0.35 g, 5 mol equiv) was added. The mixture was refluxed under argon for 8 h. Then the solvent was removed under reduced pressure and the residue was purified by flash chromatography (EtOAc/MeOH, 8:2) to afford compound **14** as a pale-yellow solid (0.13 g, 64%): mp 178−180 °C; ^{1}H NMR (DMSO-d_6) δ 3.31 (m, 2H), 3.65 (s, 2H), 4.37−4.43 (m, 4H), 6.50 (m, 1H), 7.19 (m, 6H), 7.33 (d, 2H, $J = 5.3$), 7.54 (d, 2H, $J = 6$), 8.08 (s, 1H), 8.25 (d, 1H), 9.2 (bs, 1H), 11.39 (s, 1H). Anal.($C_{26}H_{23}N_9O_3$) C, H, N.

General Procedure for Compounds 16−18: O-Debenzylation. To a solution of compounds **13−15** (0.4 mmol) in dry acetone (20 mL) was added HCO_2NH_4 (8 mol equiv) and 10% Pd/C (0.5 mmol), and the resulting mixture was heated at reflux for 12 h. The solution was cooled, and the catalyst was removed by filtration. The solvent was evaporated at reduced pressure, and the residue was washed with water (25 mL). The aqueous layer was extracted with EtOAc (3 × 20 mL), and the recombined organic phases were dried (Na_2SO_4) and evaporated under reduced pressure. The residue was purified by flash chromatography (EtOAc/MeOH, 8:2) to afford compounds **16−18**.

Biology Experiments. All synthesized compounds have been tested for their affinity to human A_1, A_{2A}, A_{2B}, and A_3 adenosine receptors. Beyond the three compounds suggested by the computational studies we also tested compounds **13−15**, and they showed quite good activity (see Table 10). The affinity values were determined by receptor binding assays at human A_1, A_{2A}, A_{2B}, and A_3 adenosine receptor subtypes cloned in Chinese hamster ovary (CHO) cells using [^{3}H]DPCPX, [^{3}H]ZM 241385, [^{3}H]MRE 2029F20, and [^{3}H]MRE 3008F20, respectively. Bound and free radioactivity were separated by rapid filtration through Whatman GF/B glass-fiber filters that were washed three times with ice-cold buffer. The filter bound radioactivity was counted in a Beckman LS-1800 spectrometer (efficiency of 55%).

Human Cloned Adenosine Receptor Binding Assay. The cells were grown and maintained in Dulbecco's modified Eagle's medium with nutrient mixture F12 without nucleosides at 37 °C in 5% CO_2/95% air. The cells were washed with phosphate-buffered saline and scraped from flasks in ice-cold hypotonic buffer (5 mM Tris-HCl, 2 mM EDTA, pH 7.4). The cell suspension was homogenized with a Polytron, and the homogenate was centrifuged

Table 10. Affinity Values of Compounds 13−15

compd	K_i (nM)			
	$hA_1{}^a$	$hA_{2A}{}^b$	$hA_{2B}{}^c$	$hA_3{}^d$
13	>1000	>1000	>1000	27 (23−32)
	(71%)	(97%)	(65%)	
14	>1000	>1000	>1000	14 (12−16)
	(74%)	(89%)	(66%)	
15	>1000	>1000	>1000	9.0 (8.1−9.9)
	(85%)	(82%)	(58%)	

^{a} Displacement of specific [^{3}H]DPCPX binding at human A_1 receptors expressed in CHO cells. ^{b} Displacement of specific [^{3}H]ZM 241385 binding at human A_{2A} receptors expressed in CHO cells. ^{c} Displacement of specific [^{3}H]MRE 2029F20 binding at human A_{2B} receptors expressed in CHO cells. ^{d} Displacement of specific [^{3}H]MRE 3008F20 binding at human A_3 receptors expressed in CHO cells.

for 30 min at 48000g. The membrane pellet was resuspended in 50 mM Tris-HCl buffer at pH 7.4 for A_1 adenosine receptors, in 50 mM Tris-HCl, 10 mM $MgCl_2$ at pH 7.4 for A_{2A} adenosine receptors, and in 50 mM Tris HCl, 10 mM $MgCl_2$, 1 mM EDTA at pH 7.4 for A_3 adenosine receptors.

Binding of [^{3}H]DPCPX to CHO cells transfected with the human recombinant A_1 adenosine receptor was performed according to the method previously described by Varani et al.[60] Displacement experiments were performed for 120 min at 25 °C in 200 μL of buffer containing 1 nM [^{3}H]DPCPX, 20 μL of diluted membranes (50 μg of protein/assay), and at least six to eight different concentrations of examined compounds. Nonspecific binding was determined in the presence of 10 μM of CHA, and this is always ≤10% of the total binding.

Binding of [^{3}H]ZM 241385 to CHO cells transfected with the human recombinant A_{2A} adenosine receptors (50 μg of protein/assay) was performed according to Varani et al.[60] In competition studies, at least six to eight different concentrations of compounds were used and nonspecific binding was determined in the presence of 1 μM ZM 241385 for an incubation time of 60 min at 25 °C.

Binding of [^{3}H]MRE 2029F20 cells transfected with the human recombinant A_{2B} adenosine receptors was performed essentially with the method described by Varani et al.[60] In particular, assays were carried out for 60 min at 25 °C in 100 μL of 50 mM Tris-HCl buffer, 10 mM $MgCl_2$, 1 mM EDTA, 0.1 mM benzamidine, pH 7.4, 2 IU/mL adenosine deaminase containing 40 nM [^{3}H]MRE 2029F20, diluted membranes (20 μg of protein/assay), and at least six to eight different concentrations of tested compounds. Nonspecific binding was determined in the presence of 100 μM NECA and was always ≤30% of the total binding.

Binding of [^{3}H]MRE 3008F20 to CHO cells transfected with the human recombinant A_3 adenosine receptors was performed according to Varani et al.[60] Competition experiments were carried out in duplicate in a finale volume of 250 μL in test tubes containing 1 nM [^{3}H]MRE 3008F20, 50 mM Tris-HCl buffer, 10 mM $MgCl_2$, pH 7.4, and 100 μL of diluted membranes (50 μg protein/assay), and at least six to eight different concentrations of examined ligands for 120 min at 4 °C. Nonspecific binding was defined as binding in the presence of 1 μM of MRE3008 F20 and was about 25% of total binding.

Data Analysis. The protein concentration was determined according to a Bio-Rad method[61] with bovine albumin as a standard reference. Inhibitory binding constants, K_i, were calculated from IC_{50} according to the Cheng−Prusoff equation.[62] A weighted nonlinear least-squares curve-fitting program LIGAND[63] was used for computer analysis of saturation and inhibition experiments. Data are expressed as the geometric mean with 95% or 99% confidence limits in parentheses.

Supporting Information Available: Details of the alignment procedure of the adenosine receptors and bovine rhodopsin amino acid sequences and elemental analysis data of the newly synthesized derivatives **13**−**18**. This material is available free of charge via the Internet at http://pubs.acs.org.

References

(1) Zhou, Q. Y.; Olah, M. E.; Johnson, R. A.; Stiles, G. L.; Clivelli, O. Molecular cloning and characterization of an adenosine receptor: the A$_3$ adenosine receptor. *Proc. Natl. Acad. Sci. U.S.A.* **1992**, *89*, 7432−7436.

(2) Jacobson, K. A. Adenosine A$_3$ receptors: novel ligands and paradoxical effects. *Trends Pharmacol. Sci.* **1998**, *19*, 184−191.

(3) Van Schaick, E. A.; Jacobson, K. A.; Kim, H. O.; IJzerman, A. P.; Danhof, M. Hemodynamic effects and histamine release elicited by the selective adenosine A$_3$ receptor agonist Cl-IB-MECA in conscious rats. *Eur. J. Pharmacol.* **1996**, *308,* 311−314.

(4) Hannon, J. P.; Pfannkuche, H. J.; Fozard, J. R. A role for mast cells in adenosine A$_3$ receptor-mediated hypotension in the rat. *Br. J. Pharmacol.* **1995**, *115*, 945−952.

(5) Ramkumar, V.; Stiles, G. L.; Beaven, M. A.; Ali, H. The A$_3$AR is the unique adenosine receptor which facilitates release of allergic mediators in mast-cells. *J. Biol. Chem.* **1993**, *268*, 16887−16890.

(6) Von Lubitz, D. K. J. E.; Carter, M. F.; Deutsch, S. I.; Lin, R. C. S.; Mastropaolo, J.; Meshulam, Y.; Jacobson, K. A. The effects of adenosine A$_3$ receptor stimulation on seizures in mice. *Eur. J. Pharmacol.* **1995**, *275*, 23−29.

(7) Von Lubitz, D. K. J. E.; Lin, R. C. S.; Popik, P.; Carter, M. F.; Jacobson, K. A. Adenosine receptors: pharmacology, structure−activity relationships, and therapeutic potential. *J. Med. Chem.* **1992**, *35*, 407−422.

(8) Beaven, M. A.; Ramkumar, V.; Ali, H. Adenosine A$_3$ receptors in mast cells. *Trends. Pharmacol. Sci.* **1994**, *15*, 13−14.

(9) Baraldi, P. G.; Cacciari, B.; Romagnoli, R.; Spalluto, G.; Klotz, K. N.; Leung, E.; Varani, K.; Gessi, S.; Merighi, S.; Borea, P. A. Pyrazolo[4,3-*e*]1,2,4-triazolo[1,5-*c*]pyrimidine derivatives as highly potent and selective human A$_3$ adenosine receptor antagonists. *J. Med. Chem.* **1999**, *42*, 4473−4478.

(10) Baraldi, P. G.; Cacciari, B.; Romagnoli, R.; Spalluto, G.; Moro, S.; Klotz, K. N.; Leung, E.; Varani, K.; Gessi, S.; Merighi, S.; Borea, P. A. Pyrazolo[4,3-*e*]1,2,4-triazolo[1,5-*c*]pyrimidine derivatives as highly potent and selective human A$_3$ adenosine recptor antagonists: influence of the chain at the N^8 pyrazole nitrogen. *J. Med. Chem.* **2000**, *43*, 4768−4780.

(11) Baraldi, P. G.; Cacciari, B.; Moro, S.; Spalluto, G.; Pastorin, G.; Da Ros, T.; Klotz, K. N.; Varani, K.; Gessi, S.; Borea, P. A. Synthesis, biological activity, and molecular modeling investigation of new pyrazolo[4,3-*e*]1,2,4-triazolo[1,5-*c*]pyrimidine derivatives as human A$_3$ adenosine receptor antagonists. *J. Med. Chem.* **2002**, *45*, 770−780.

(12) Maconi, A.; Pastorin, G.; Da Ros, T.; Spalluto, G.; Gao, Z.g.; Jacobson, K. A.; Baraldi, P. G.; Cacciari, B.; Varani, K.; Moro, S.; Borea, P. A. Synthesis, biological properties, and molecular modeling investigation of the first potent, selective, and water-soluble human A3 Adenosine receptor antagonist. *J. Med. Chem.* **2002**, *45*, 3579−3582.

(13) Kim, Y. C.; Ji, X. D.; Jacobson, K. A. Derivatives of the triazoloquinazoline adenosine antagonist (CGS15943) are selective for the human A$_3$ receptor subtype. *J. Med. Chem.* **1996**, *39*, 4142−4148.

(14) Van Muijlwijk-Koezen, J. E.; Timmerman, H.; Link, R.; van der Goot, H.; IJzerman, A. P. A novel class of adenosine A$_3$ receptor ligands. 1. 3-(2-Pyridinyl)isoquinoline derivatives. *J. Med. Chem.* **1998**, *41*, 3987−3993.

(15) Van Muijlwijk-Koezen, J. E.; Timmerman, H.; Link, R.; van der Goot, H.; IJzerman, A. P. A novel class of adenosine A$_3$ receptor ligands. 2. Structure affinity profile of a series of isoquinoline and quinazoline compounds. *J. Med. Chem.* **1998**, *41*, 3994−4000.

(16) Van Muijlwijk-Koezen, J. E.; Timmerman, H.; van der Goot, H.; Menge, W. M. P. B.; von Drabbe Künzel, J. F.; de Groote, M.; Ijzerman, A. P. Isoquinoline and quinazoline urea analogues as antagonists for the human adenosine A$_3$ receptor. *J. Med Chem.* **2000**, *43*, 2227−2238.

(17) Li, A. H.; Moro, S.; Melman, N.; Ji, X. D.; Jacobson, K. A. Structure−activity relationships and molecular modeling of 3,5-diacyl-2,4-dialkylpyridine derivatives as selective A$_3$ adenosine receptor antagonists. *J. Med. Chem.* **1998**, *41*, 3186−3201.

(18) Li, A. H.; Moro, S.; Forsyth, N.; Melman, N.; Ji, X. D.; Jacobson, K. A. Synthesis, CoMFA analysis, and receptor docking of 3,5-diacyl-2,4-dialkylpyridine derivatives as selective A$_3$ adenosine receptor antagonists. *J. Med. Chem.* **1999**, *42*, 706−721.

(19) Xie, R.; Li, A. H.; Ji, X. D.; Melman, N.; Olah, M. E.; Stiles, G. L.; Jacobson, K. A. Selective A$_3$ adenosine receptor antagonists: water-soluble 3,5-diacyl-1,2,4-trialkylpiridinium salts and their oxidative generation from dihydropyridine precursors. *J. Med. Chem.* **1999**, *42*, 4232−4238.

(20) Van Rhee, A. M.; Jiang, J. L.; Melman, N.; Olah, M. E.; Stiles, G. L.; Jacobson, K. A. Interaction of 1,4-dihydropyridine and pyridine derivatives with adenosine receptors: selectivity for A$_3$ receptors. *J. Med. Chem.* **1996**, *39*, 2980−2989.

(21) Jiang, J. L.; Van Rhee, A. M.; Chang, L.; Patchornik, A.; Ji, X. D.; Evans, P.; Melman, N.; Jacobson, K. A. Structure−activity relationships of 4-(phenylethynyl)-6-phenyl-1,4-dihydropyridines as highly selective A3 adenosine receptor antagonists. *J. Med. Chem.* **1997**, *40*, 2596−2608.

(22) Jalaie, M.; Erickson, J. A. Homology model directed alignment selection for comparative molecular field analysis: Application to photosystem II inhibitors. *J. Comput.-Aided Mol. Des.* **2000**, *14*, 181−197.

(23) Bröer, B. M.; Gurrath, M.; Höltje, H. D. Molecular modelling studies on the ORL1-receptor and ORL1-agonists. *J. Comput.-Aided Mol. Des.* **2003**, *17*, 739−754.

(24) Poulsen, A.; Bjørnholm, B.; Gundertofte, K.; Pogozheva, I. D.; Liljefors, T. Pharmacophore and receptor models for neurokinin receptors. *J. Comput.-Aided Mol. Des.* **2003**, *17*, 765−783.

(25) Pogozheva, I. D.; Przydzial, M. J.; Mosberg, H. J. Homology modeling of opioid receptor−ligand complexes using experimental constraints. *Am. Assoc. Pharm. Sci. J.* **2005**, *7*, E434−E448 and references therein.

(26) Evers, A.; Gohlke, H.; Klebe, G. Ligand supported homology modelling of protein binding-sites using knowledge-based potentials. *J. Mol. Biol.* **2003**, *334*, 327−345.

(27) Evers, A.; Klebe, G. Ligand-supported homology modelling of G-protein coupled receptor sites: Models sufficient for successful virtual screening. *Angew. Chem., Int. Ed.* **2004**, *43*, 248−251.

(28) Di Santo, R.; Tafi, A.; Costi, R.; Botta, M.; Artico, M.; Corelli, F.; Forte, M.; Caporuscio, F.; Angiolella, L.; Palamara, A. T. Antifungal agents. 11. N-Substituted Derivatives of 1-[(aryl)(4-aryl-1*H*-pyrrol-3-yl)methyl]-1*H*-imidazole: Synthesis, anti-Candida activity, and QSAR studies. *J. Med. Chem.* **2005**, *48*, 3019−3031.

(29) Ferrarini, P. L.; Betti, L.; Cavallini, T.; Giannaccini, G.; Lucacchini, A.; Manera, C.; Martinelli, A.; Ortore, G.; Saccomanni, G.; Tuccinardi, T. Study on affinity profile toward native human and bovine adenosine receptors of a series of 1,8-naphthyridine derivatives. *J. Med. Chem.* **2004**, *47*, 3019−3031.

(30) Palczewski, K.; Kumasaka, T.; Hori, T.; Behnke, C. A.; Motoshima, H.; Fox, B. A.; Le Trong, I.; Teller, D. C.; Okada, T.; Stenkamp, R. E.; Yamamoto, M.; Miyano, M. Crystal structure of rhodopsin: A G protein-coupled receptor. *Science* **2000**, *289*, 739−745.

(31) Moro, S.; Li, A. H.; Jacobson, K. A. Molecular modeling studies of A$_3$ adenosine antagonists: structural homology and receptor docking. *J. Chem. Inf. Comput. Sci.* **1998**, *38*, 1239−1248.

(32) *Catalyst 4.6*; Accelrys, Inc. (9685 Scranton Road, San Diego, CA 92121).

(33) Catalyst 4.6 manual at http://www.accelrys.com.

(34) GPCRDB: Information System for G Protein-coupled receptors (GPCRs). www.gpcr.org.

(35) Thompson, J. D.; Higgins, D. G.; Gibson, T. J. CLUSTAL W: improving the sensitivity of progressive multiple sequence alignment through sequence weighting, position-specific gap penalties and weight matrix choice. *Nucleic Acids Res.* **1994**, *22*, 4673−4680.

(36) Fredriksson, R.; Lagerström, M. C.; Lundin, L. G.; Schiöth, H. B. The G-protein-coupled receptors in the human genome form five main families. Phylogenetic analysis, paralogon groups, and fingerprints. *Mol. Pharmacol.* **2003**, *63*, 1256−1272.

(37) Gouldson, P. R.; Snell, C. R.; Reynolds, C. A. A new approach to docking in the β2-adrenergic receptor that exploits the domain structure of G-protein-coupled receptors. *J. Med. Chem.* **1997**, *40*, 3871−3886.

(38) Cruciani, G.; Goodford, P. *GREATER Graphical Interface for GRID,* version, 1.1.7 GRIB, UPF/IMIM; Molecular Discovery Ltd.: Barcelona, Spain, 2001−2003; http://www.moldiscovery.com.

(39) Chen, A.; Gao, Z. G.; Barak, D.; Liang, B. T.; Jacobson, K. A. Constitutive activation of A$_3$ adenosine receptors by site-directed mutagenesis. *Biochem. Biophys. Res. Commun.* **2001**, *284*, 596−601.

(40) Gao, Z. G.; Chen, A.; Barak, D.; Kim, S. K.; Muller, C. E.; Jacobson, K. A. Identification by site-directed mutagenesis of residues involved in ligand recognition and activation of the human A$_3$ adenosine receptor. *J. Biol. Chem.* **2002**, *277*, 19056−19063.

(41) Gao, Z. G.; Kim, S. K.; Biadatti, T.; Chen, W.; Lee, K.; Barak, D.; Kim, S. G.; Johnson, C. R.; Jacobson, K. A. Structural determinants of A3 adenosine receptor activation: nucleoside ligands at the agonist/antagonist boundary. *J. Med. Chem.* **2002**, *45*, 4471−4484.

(42) Jacobson, K. A.; Gao, Z. G.; Chen, A.; Barak, D.; Kim, S. A.; Lee, K.; Link, A.; Van Rompaey, P.; Van Calenberg, S.; Liang, B. T. Neoceptor concept based on molecular complementarity in GPCRs: a mutant adenosine A3 receptor with selectively enhanced affinity for amine-modified nucleosides. *J. Med. Chem.* **2001**, *44*, 4125−4136.

(43) Morris, G. M.; Goodsell, D. S.; Halliday, R. S.; Huey, R.; Hart, W. E.; Belew, R. K.; Olson, A. J. Automated docking using a Lamarckian genetic algorithm and empirical binding free energy function. *J. Comput. Chem.* **1998**, *19*, 1639−1662.

(44) Costantino, G.; Macchiarulo, A.; Campioni, E.; Pellicciari, R. Modeling of poly(ADP-ribose)polymerase (PARP) inhibitors. Docking of ligands and quantitative structure−activity relationship analysis. *J. Med. Chem.* **2001**, *44*, 3786−3794.

(45) Tanczos, A. C.; Palmer, R. A.; Potter, B. S.; Saldanha, J. W.; Howlin, B. J. Antagonist binding in the rat muscarinic receptor. A study by docking and X-ray crystallography. *Comp. Biol. Chem.* **2004**, *28*, 375−385.

(46) Tuccinardi, T.; Ferrarini, P. L.; Manera, C.; Ortore, G.; Saccomanni, G.; Martinelli, A. Cannabinoid CB2/CB1 selectivity. Receptor modeling and automated docking analysis. *J. Med. Chem.* **2006**, *49*, 984−994.

(47) Baraldi, P. G.; Cacciari, B.; Moro, S.; Romagnoli, R.; Ji, X.; Jacobson, K. A.; Gessi, S.; Borea, P. A.; Spalluto, G. Fluorosulfonil- and bis-(β-chloroehyl)amino-phenylamino functionalized pyrazolo[4,3-*e*]1,2,4-triazolo[1,5-*c*]pyrimidine derivatives: irreversible antagonists at the human A3 adenosine receptor and molecular modelling studies. *J. Med. Chem.* **2001**, *44*, 2735−2742.

(48) Baraldi, P. G.; Bovero, A.; Fruttarolo, F.; Romagnoli, R.; Tabrizi, M. A.; Preti, D.; Varani, K.; Borea, P. A.; Moorman, A. R. New strategies for the synthesis of A3 adenosine receptor antagonists. *Bioorg. Med. Chem.* **2003**, *11*, 4161−4169.

(49) Singha, C. N.; Dixit, N.; Sathyanarayana, D. N. ^{1}H and ^{13}C NMR spectra of some asymmetric *N,N*-dipyridyl ureas: spectral assignments and molecular conformations. *J. Chem. Soc., Perkin Trans. 2* **1997**, 157−162.

(50) Curtius, T.; Mohr, E. Transformation of nicotinic acid to beta-aminopyridine. *Ber.* **1898**, *31*, 2493−2495.

(51) Smellie, A.; Teig, S.; Towbin, P.; Poling, P. Promoting conformational variation. *J. Comput. Chem.* **1995**, *16*, 171−187.

(52) Case, D. A.; Pearlman, D. A.; Caldwell, J. W.; Cheatham, T. E., III; Ross, W. S.; Simmerling, C. L.; Darden, T. A.; Merz, K. M.; Stanton, R. V.; Cheng, A. L.; Vincent, J. J.; Crowley, M.; Tsui, V.; Radmer, R. J.; Duan, Y.; Pitera, J.; Massova, I.; Seibel, G. L.; Singh, U. C.; Weiner, P. K.; Kollman, P. A. *AMBER 6*; University of California: San Francisco, CA, 1999.

(53) *MacroModel*, version 7.2; Schrodinger Inc., 1999; http://www.schroedinger.com.

(54) Pearlman, D. A.; Case, D. A.; Caldwell, J. W.; Ross, W. S.; Cheatham, T. E., III; Ferguson, D. M.; Seibel, G. L.; Chandra Singh, U.; Weiner, P. K.; Kollman, P. A. *AMBER 4.1*; University of California: San Francisco, CA, 1995.

(55) *InsightII (98) Molecular Modeling System, MSI*; Accelrys Software, Inc.; http://www.accelrys.com.

(56) Huang, C. C.; Couch, G. S.; Pettersen, E. F.; Ferrin, T. E. Chimera: an extensible molecular modelling application constructed using standard components. *Pac. Symp. Biocomput.* **1996**, *1*, 724; http://www.cgl.ucsf.edu/chimera.

(57) *WebLab Viewer Pro 3.7*; Accelrys Inc.: San Diego, CA.

(58) Fiser, A.; Do, R. K.; Sali, A. Modeling of loops in protein structures. *Protein Sci.* **2000**, *9* 1753−1773.

(59) Hyden, S.; Wilbert, G. Pyridine isocyanates. *Chem. Ind. (London)* **1967**, *33*, 1406−1407.

(60) Varani, K.; Merighi, S.; Gessi, S.; Klotz, K. N.; Leung, E.; Baraldi, P. G.; Cacciari, B.; Romagnoli, R.; Spalluto, G.; Borea, P. A. [^{3}H]-MRE 3008F20: A novel radioligand for the pharmacological and biochemical characterization of human A3 adenosine receptors. *Mol. Pharmacol.* **2000**, *57*, 968−975.

(61) Bradfor, M. M. A rapid and sensitive method for the quantification of microgram quantities of protein utilizing the principle of protein dye-binding. *Anal. Biochem.* **1976**, *72*, 248−254.

(62) Cheng, Y. C.; Prusoff, W. H. Relationship between the inhibition constant (K_i) and the concentration of inhibitor which causes 50% inhibition (IC_{50}) of an enzymatic reaction. *Biochem. Pharmacol.* **1973**, *22*, 3099−3108.

(63) Munson, P. J.; Rodbard, D. Ligand: a versatile computerized approach for the characterization of ligand binding system. *Anal. Biochem.* **1980**, *107*, 220−239.

JM051112+